



Article

Formation and Antibacterial Activity of AlOOH/Ag Composite Coating on Macroporous α -Al₂O₃ Ceramics

Elena I. Senkina, Ales S. Buyakov , Sergey O. Kazantsev, Olga V. Bakina, Maksim G. Krinitsyn 
and Aleksandr S. Lozhkomoev *

Laboratory of Nanobioengineering, Institute of Strength Physics and Materials Science of Siberian Branch of Russian Academy of Sciences (ISPMS SB RAS), 2/4, pr. Akademicheskii, 634055 Tomsk, Russia; elena.senkina.1995@mail.ru (E.I.S.); alesbuyakov@gmail.com (A.S.B.); kzso@ispms.tsc.ru (S.O.K.); ovbakina@ispms.tsc.ru (O.V.B.); krinmax@gmail.com (M.G.K.)

* Correspondence: asl@ispms.tsc.ru

Abstract: In this study, the modification of macroporous α -Al₂O₃ ceramics with AlOOH nanostructures impregnated with silver particles is carried out using bicomponent Al/Ag nanoparticles obtained by the simultaneous electrical explosion of Al and Ag wires. Nanoparticle suspension impregnation of porous ceramics followed by oxidation with water is shown to lead to the formation of a continuous AlOOH nanosheet coating on the ceramic surface, with silver releasing on the surface of nanosheets in the form of individual particles sized 5–30 nm. Modified with AlOOH/Ag nanostructures, macroporous α -Al₂O₃ pellets with a diameter of 11 mm and a thickness of 5 mm show 100% efficiency for water purification from bacteria with a concentration of 10⁵ CFU/mL for 7.5 min at a flow rate of 6.7 mL/min.

Keywords: macroporous ceramics; modification; nanoparticles; oxidation; nanosheets; nanostructured coating; boehmite; antimicrobial activity



Citation: Senkina, E.I.; Buyakov, A.S.; Kazantsev, S.O.; Bakina, O.V.; Krinitsyn, M.G.; Lozhkomoev, A.S. Formation and Antibacterial Activity of AlOOH/Ag Composite Coating on Macroporous α -Al₂O₃ Ceramics. *Coatings* **2022**, *12*, 1107. <https://doi.org/10.3390/coatings12081107>

Academic Editor: Jean-François Berret

Received: 22 June 2022

Accepted: 31 July 2022

Published: 3 August 2022

Publisher's Note: MDPI stays neutral with regard to jurisdictional claims in published maps and institutional affiliations.



Copyright: © 2022 by the authors. Licensee MDPI, Basel, Switzerland. This article is an open access article distributed under the terms and conditions of the Creative Commons Attribution (CC BY) license (<https://creativecommons.org/licenses/by/4.0/>).

1. Introduction

Macroporous ceramic materials are widely used as particulate filters, hot gas filters, water purification filters, catalyst carriers, bone implants, etc. [1–5]. These applications are due to a set of properties inherent in such materials, among which are a high melting point [6], hardness and strength [7], wear resistance [8], chemical stability [9], and bioinertness [10].

The most typical representative of macroporous ceramics is Al₂O₃ (alumina). A variety of applications of alumina-based ceramic materials are available due to its high strength and stability resulting from strong ionic and covalent bonds, as well as a high surface area which allows the production of highly porous materials [11]. Alumina-based ceramics are used in the production of catalyst carriers [12–14], membrane materials [15–20], gas–liquid filters [21,22], and sensor materials [23].

However, even with all the above advantages, porous ceramics often need surface modification, which can be realized by adding various functional groups [24–26] or by the attachment of nanoparticles [27–32]. Surface modification can improve the sorption and selective efficiency and antimicrobial and photochemical properties, as well as the catalytic activity of the porous ceramic materials.

Ceramics surfaces can be modified with nanoparticles formed by physical or chemical vapor deposition, laser cladding, sol–gel method, etc. [33,34]. However, not all methods are suitable for the surface modification of porous ceramics. As a rule, wet chemistry methods are used for this purpose by performing chemical reactions on the ceramic surface [35]. This concerns both the reduction of silver salts on the ceramic surface [36,37] and the synthesis of complex nanostructures by sol–gel methods [38], chemical grafting [39], and immersion methods [40].

The water oxidation of Al/Ag nanoparticles, including those fixed on the macroparticle outermost surface, yields boehmite nanosheet structures with highly specific surface areas of up to 300 m²/g, decorated with silver nanoparticles of 5–30 nm in size [41,42]. This approach can be used to modify macroporous alumina ceramics by impregnation in the suspension of Al/Ag nanoparticles followed by the oxidation of the nanoparticles fixed in the pore space.

In the present work, for the first time, nanostructured AlOOH/Ag composite coatings are obtained on the surface of macroporous alumina ceramics using electroexplosive Al/Ag nanoparticles, which contribute to an increase in antimicrobial activity.

2. Materials and Methods

2.1. Preparation of Alumina Macroporous Ceramics

The initial ceramic composition was obtained by the mechanical mixing of Al₂O₃ nanopowder (Advanced Powder Technologies LLC, Tomsk, Russia) with a porogenic agent as irregularly shaped rosin particles sized 300–500 µm, with the rosin particle content being 80 vol.%. The initial ceramic composition weight, about 0.5 g, was pressed in a steel mold under a pressure of 130 MPa. The removal of the porogen agent was carried out by annealing the pressed samples in a muffle furnace (Naberterm LHT 08/18/3310 (Naberterm, Lilienthal, Germany) at 1100 °C with isothermal dwelling for 1 h. To sinter the ceramic material the temperature was increased to 1600 °C and kept for 1 h.

2.2. Preparation of Al and Al/Ag Nanoparticles

Al and Al/Ag nanoparticles were obtained by the electrical explosion of Al wires and twisted Al and Ag wires, respectively, in an argon atmosphere according to the methods reported previously [43,44]. The Al/Ag ratio of the bi-metallic nanoparticles was determined by the ratio of metals in the exploded wires. In this work, a twist of two Al wires with a diameter of 0.35 mm and an Ag wire with a diameter of 0.15 mm was used, corresponding to the Ag content in the prepared nanoparticles of about 8.4 at. %.

2.3. Formation of a Composite AlOOH/Ag Coating on the Surface of α -Al₂O₃ Ceramics

A suspension with Al or Al/Ag nanoparticle content of 1 wt.% in ethanol was prepared using an ultrasonic bath. After that, alumina macroporous ceramic disks weighing about 0.5 g were immersed in the suspension and impregnated for 30 min under constant ultrasonic irradiation. Then, the samples prepared were removed from the suspension and dried for 30 min at 60 °C. The dried samples were placed in a reactor with 10 mL of deionized water preheated to 60 °C and held for 1 h. During the interaction of aluminum and water, the amount of hydrogen released was recorded from the displaced volume of liquid in the communicating vessel system. After the reaction was complete, the samples were removed and dried at 120 °C for 2 h. The amount of immobilized nanoparticles on the alumina ceramics was determined by the sample mass gain and the amount of released hydrogen.

2.4. Characterization of Research Objects

Nanoparticles and porous composites were characterized using an XRD-6000 diffractometer (Shimadzu, Kyoto, Japan) with CuK α radiation. X-ray diffraction was carried out using the PCPDFWIN database as well as the PowderCell 2.4 software package (W. Kraus & G. Nolze, Berlin, Germany). The morphology and elemental composition of the nanoparticles and nanostructures were characterized by transmission electron microscopy (TEM) using a JEM-2100 microscope (JEOL, Tokyo, Japan) with an integrated energy-dispersive X-Ray spectroscopy (EDS) system X-Max (Oxford Instruments, Abingdon, UK). The average nanoparticle size was determined from the TEM data, and histograms of the nanoparticle size distribution were constructed using the sizes of at least 1500 particles measured.

The surface morphology of the composites before and after modification was studied by scanning electron microscopy (SEM) using an LEO EVO 50 electron microscope (Carl

Zeiss AG, Jena, Germany) equipped with an INCA-Energy 450 EDS analyzer (Oxford Instruments, Abingdon, UK).

2.5. Antibacterial Assay

Staphylococcus aureus ATCC 6538-R bacterial culture was used to determine the antimicrobial activity of the porous ceramic samples. Using a single-channel peristaltic pump (JSC LOIP, Saint-Petersburg, Russia), 100 mL of deionized water containing 10^5 CFU/mL of bacteria was pumped through the fixed sample of 11 mm in diameter and 5 mm in thickness at a rate of 6.7 mL/min. Filtrate samples were taken in sterile 10 mL tubes; then, 20 μ L was taken from each sample, diluted 10-fold, and 20 μ L was inoculated on nutrient agar into Petri dishes using the track method. Incubation was performed at 37 °C for 24 h in a Binder APT line™ series BF 115 thermostat (Binder, Tuttlingen, Germany). Colonies were counted using the Scienceware® colony counting system (SP Scienceware, Pequannock, NJ, USA). The bacterial concentration in the filtrate was determined by taking into account the dilutions used in the experiment.

3. Results and Discussion

Al and Al/Ag nanopowders were used to form AlOOH and AlOOH/Ag nanostructured coatings on the surface of macroporous alumina ceramics. Figure 1 shows TEM images of the nanoparticles used and their size distribution. The particles had a spherical shape and were covered with an oxide layer 4–5 nm thick. The nanopowders were characterized by a lognormal particle size distribution with the average size of Al nanoparticles being 89 ± 1.4 nm and Al/Ag nanoparticles being 96 ± 0.7 nm (Figure 1c).

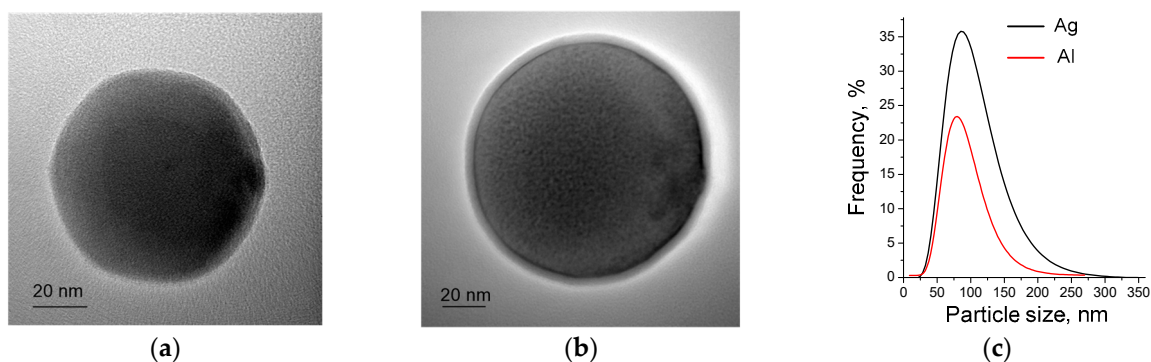


Figure 1. TEM images of the Al (a) и and Al/Ag (b) nanoparticles and nanoparticle size distribution curve (c).

The peaks of the diffraction pattern (Figure 2a) correspond to planes 111, 200, 220, 311 and 222 in accordance with a powder diffraction file of the International Centre for Diffraction Data (ICDD), card No. 00-004-0787. In both cases, the lattice parameters are standard for aluminum and are 4.049 Å. According to the conventional Williamson–Hall plot, the crystallite size for Al/Ag nanoparticles is smaller than that for Al nanoparticles and is 40 ± 2 nm versus 55 ± 2 nm. The absence of Ag peaks in the diffraction pattern of Al/Ag nanoparticles may be due to its distribution in the particles in the form of X-ray amorphous clusters (Guinier–Preston zones). This phenomenon is associated with the formation of an oversaturated Al-based solid solution [45] and is characterized by the extremely small size of Ag clusters [46–50].

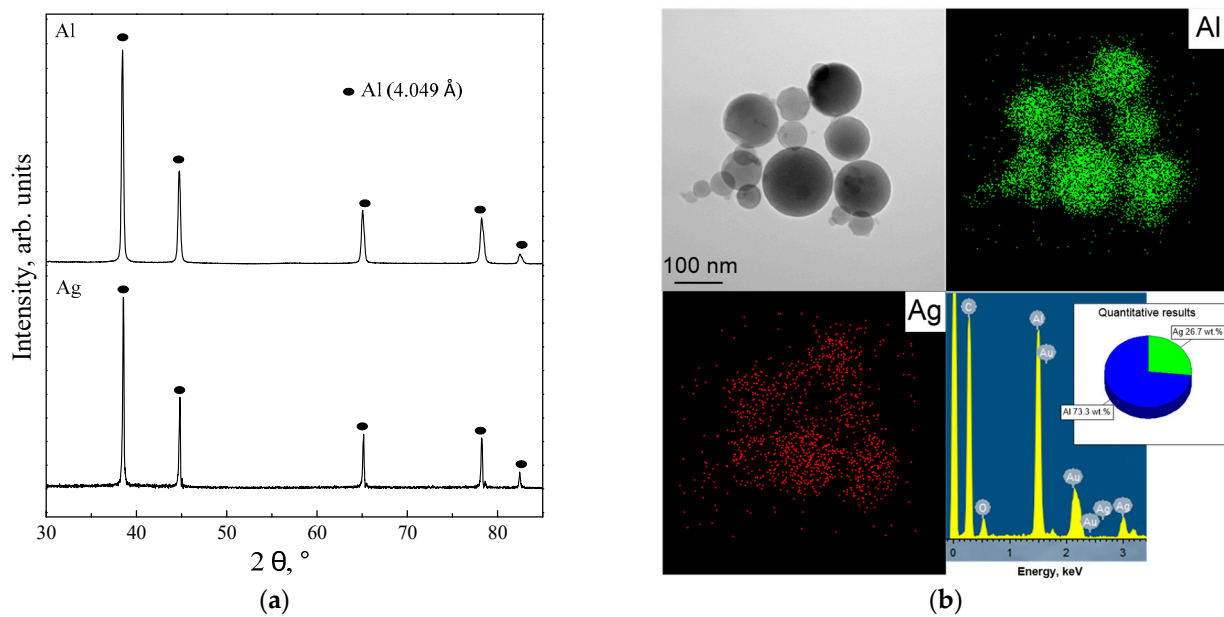


Figure 2. Diffraction pattern of Al and Al/Ag nanoparticles (a) and TEM-EDS and elemental distribution maps of Al/Ag nanoparticles (b).

The presence of silver in the nanoparticles was confirmed by TEM-EDS analysis (Figure 2b). In the TEM-EDS images obtained in the mapping mode, Al and Ag were distributed within the nanoparticles. The weight ratio of Al to Ag in the sample corresponded to that of metals in the wires exploded, being 73 and 27 wt.%, respectively. The presence of Au and C in the spectrum (Figure 2b) was due to the use of formvar/carbon-coated Au TEM grids.

The properties of Al and Al/Ag nanoparticles, as well as the features of the nanoparticle-water interaction, have been described in detail previously [51,52].

The macroporous ceramic samples were prepared in the form of 11 mm diameter discs with a thickness of 5 mm (Figure 3a). To obtain AlOOH and AlOOH/Ag coatings on the surface of the macroporous ceramics, they were pre-impregnated in 1 wt.% Al or Al/Ag nanopowder suspension in order to fix the nanoparticles on the surface (Figure 3b). An open pore system of high porosity and pore size are important for the complete impregnation of porous ceramics. In this case, the porosity of the alumina ceramic samples was 75% with an average pore size of $187.2 \pm 2.5 \mu\text{m}$ (Figure 3c).

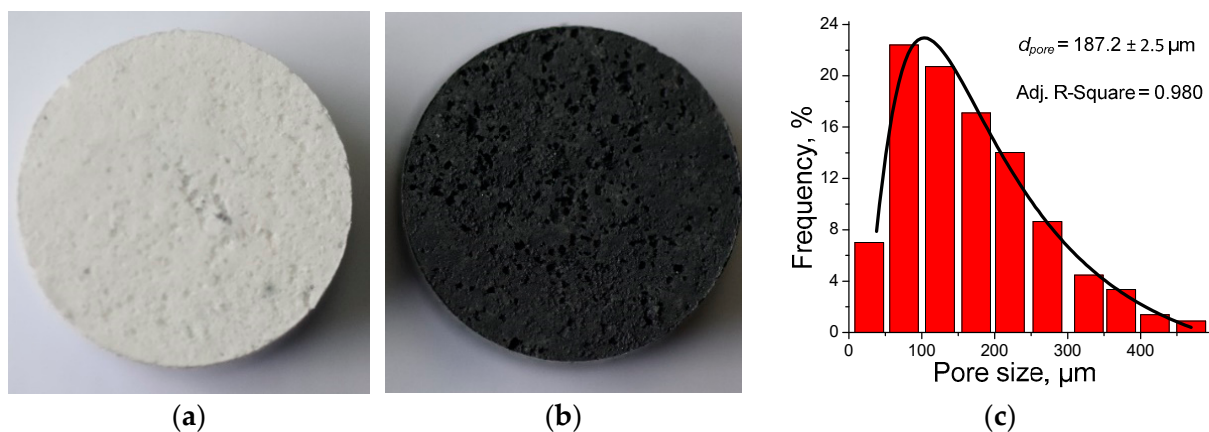


Figure 3. Images of the macroporous ceramic samples before (a) and after (b) impregnation with Al or Al/Ag nanoparticle suspension and pore size distribution curve (c). The disc diameter is 11 mm.

The amount of hydrogen released as a result of the aluminum–water interaction was used as an estimate of the amount of fixed nanoparticles on the ceramics (Figure 4). The obtained kinetic dependences had an S-shape form typical for hydrogen release during the water oxidation of Al powders [53]. Hydrogen release began after an about 10 min delay and was completed after 30 min both in the case of the oxidation of Al nanoparticles and in the case of the oxidation of Al/Ag nanoparticles. The reaction of the fixed Al nanoparticles with water resulted in the release of 9.4 mL of hydrogen, while the oxidation of Al/Ag nanoparticles resulted in the release of 5.3 mL. These amounts of hydrogen were released upon the complete oxidation of 7.5 mg and 4.2 mg of aluminum, respectively.

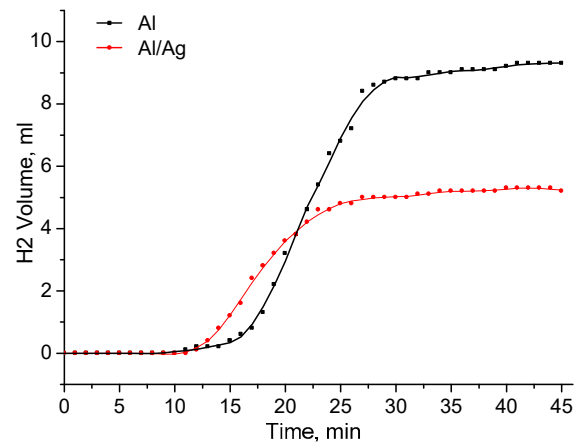


Figure 4. Hydrogen release kinetics during water oxidation of Al (black curve) and Al/Ag nanoparticles (red curve) fixed at the alumina ceramics surface.

Figure 5 shows SEM images of the ceramic surface before and after modification. As can be seen, the pristine ceramic surface had multiple pores, and the ceramic structure was represented by grains with an average size of $5.1 \pm 0.6 \mu\text{m}$ (Figure 5a). After ceramic modification by the water oxidation of Al and Al/Ag nanoparticles fixed on its surface, the formation of continuous porous coating and separate agglomerates of about $1 \mu\text{m}$ size was observed (Figure 5b,c). The agglomerates had a nanosheet structure similar to that formed as a result of the water oxidation of Al and Al/Ag nanopowder [41,52] (Figure 5b,c inset).

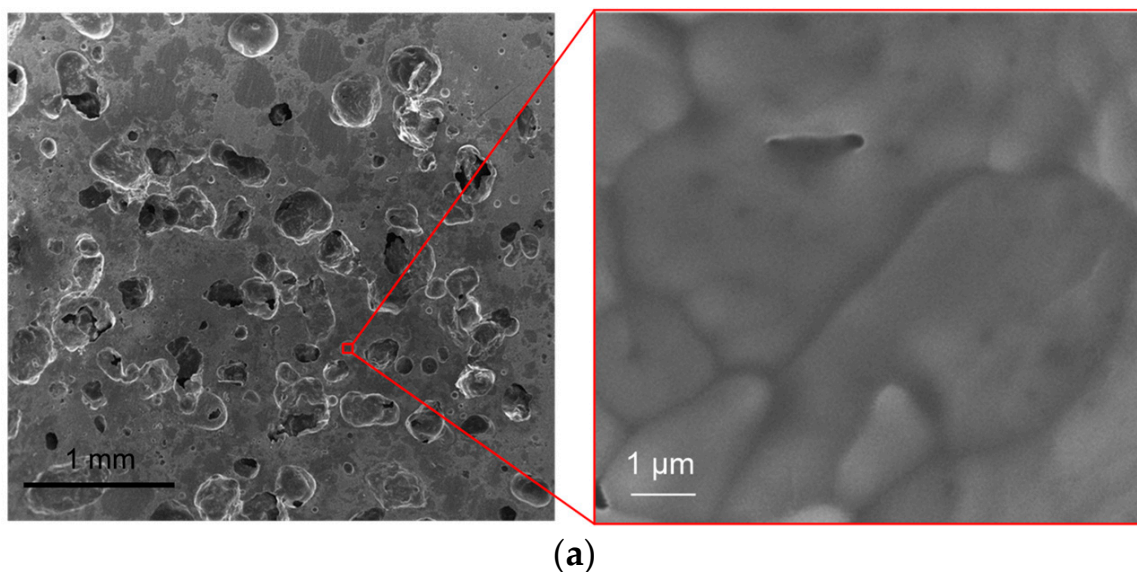


Figure 5. Cont.

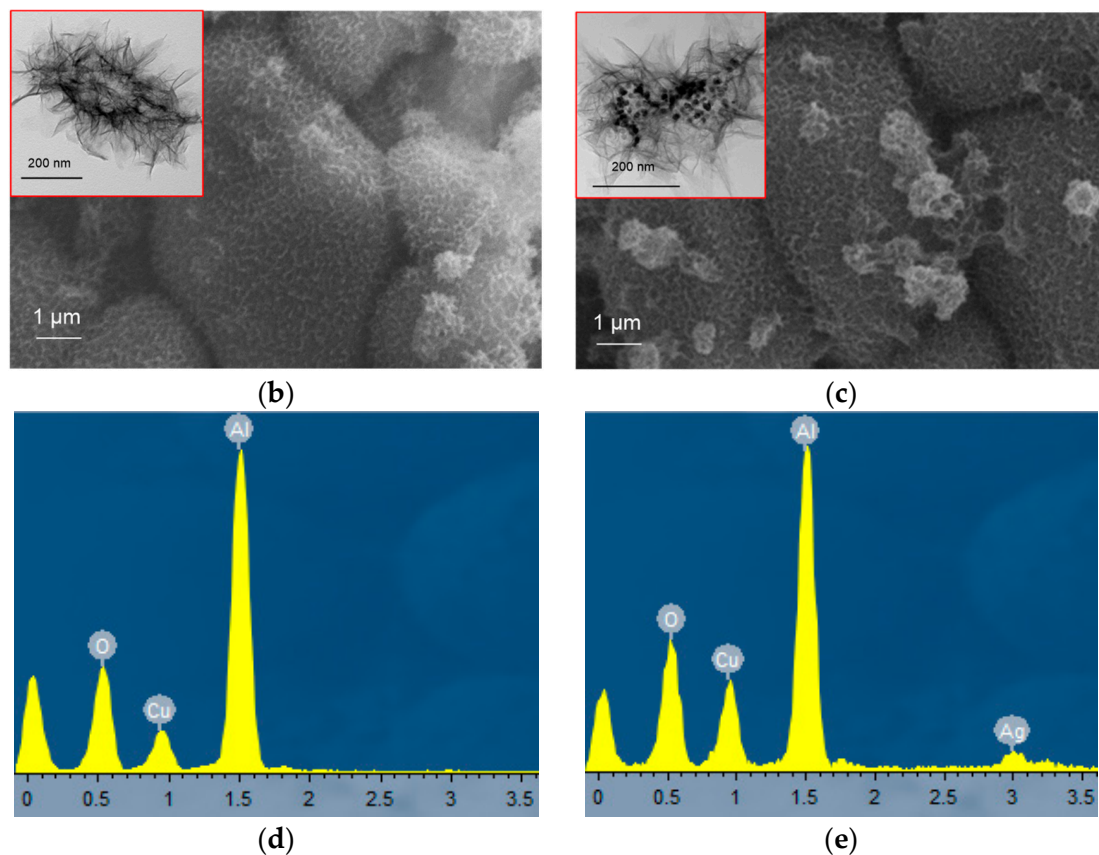


Figure 5. SEM images of macroporous alumina ceramic before (a) and after modification with AIOOH (b) and AIOOH/Ag (c) nanostructures; EDX spectra of the ceramics surface after the modification with AIOOH (d) and AIOOH/Ag (e) nanostructures. Insets in (b,c) images show nanostructures formed by water oxidation of Al and Al/Ag nanoparticles under similar conditions.

Elemental analysis of the modified samples' surfaces indicated the presence of silver in the case of ceramic modification by the oxidation products of Al/Ag nanoparticles (Figure 5e).

As a result of the modification of porous ceramics by AIOOH/Ag nanostructures, silver was distributed over the entire surface, and its content according to SEM-EDS analysis relative to Al and O was 1.5 ± 0.4 wt.% (Figure 6). According to our previous works, the oxidation of Al/Ag nanoparticles by water yields boehmite nanosheet structures with silver particles 5–30 nm in size fixed on the nanosheet surface [41]. It should be expected that similar regularities are preserved during the oxidation of Al/Ag nanoparticles on the surface of alumina ceramics.

According to the XRD phase analysis (Figure 7), the main diffraction peaks in the patterns of the studied samples corresponded to α - Al_2O_3 —corundum (ICDD card No. 00-004-0787). The lattice parameters of the pristine α - Al_2O_3 ceramics slightly differed from those of the ceramics modified with AIOOH and AIOOH/Ag nanostructures, at 4.7587 Å, 4.7562 Å and 4.7559 Å, respectively, which agrees with the values reported [54]. The value of the coherent scattering regions (d_{CSR}) determined by the Williamson–Hall method for all samples was about 80 nm. The absence of the diffraction peaks corresponding to AIOOH was due to its low crystallinity [55] and its low content in the sample. The absence of silver diffraction peaks was due to the low content of noble metal particles in the sample.

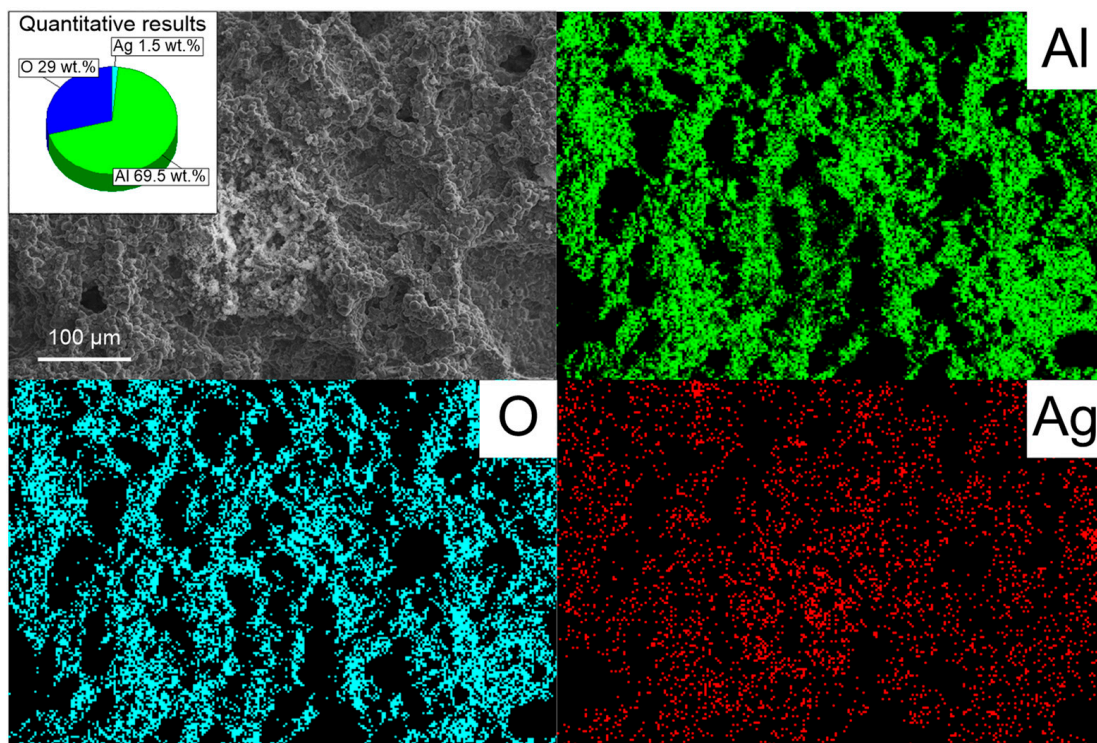


Figure 6. SEM image and elemental mapping EDS analysis of the macroporous ceramics surface modified with AlOOH/Ag nanostructures.

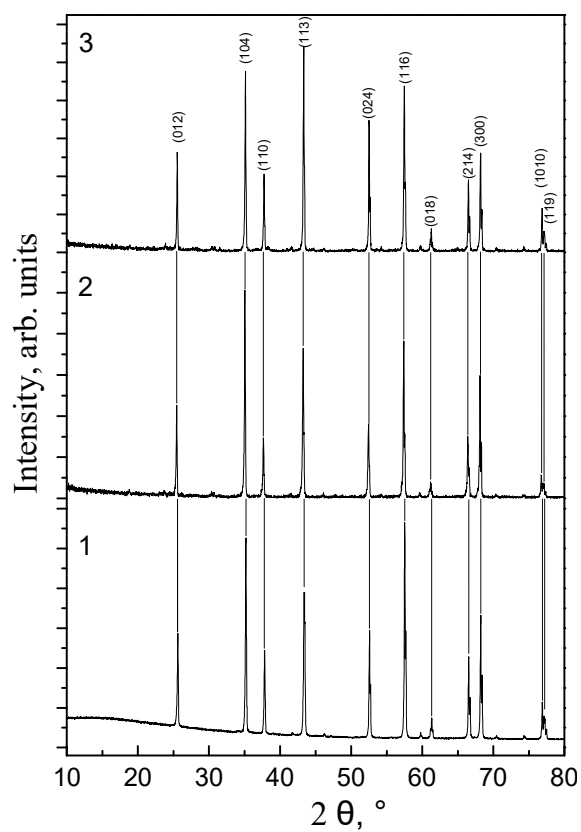


Figure 7. XRD pattern of pristine α -Al₂O₃ ceramic (1), α -Al₂O₃ ceramic modified with AlOOH (2) and AlOOH/Ag (3) nanostructures.

Figure 8 shows the efficiency of *S. aureus* removal from water as a function of the water volume passed through the macroporous ceramic samples. When passing 100 mL of water with a bacterial concentration of 10^5 CFU/mL through the pristine macroporous ceramics, the removal efficiency was 76% (Figure 8, curve 1). The modification of the ceramics with AlOOH nanostructures led to an increase in removal efficiency of up to 89% (Figure 8, curve 2), and when modified with AlOOH/Ag (Figure 8, curve 3) nanostructures, the efficiency was 98%. At the same time, for the sample containing silver, the removal efficiency after passing 50 mL of contaminated water was 100%.

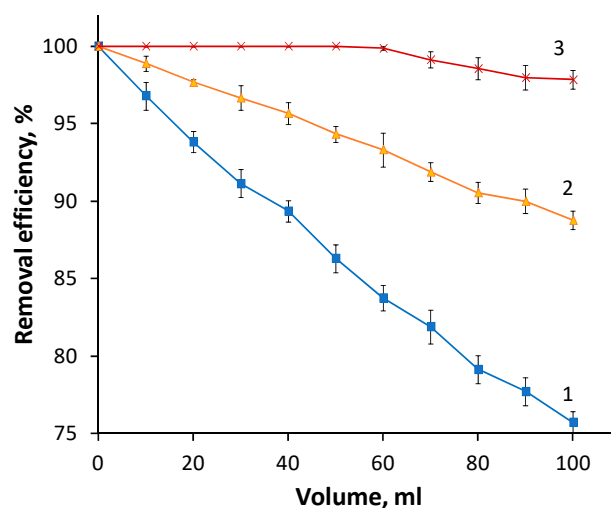


Figure 8. Efficiency of *S. aureus* removal from water as a function of the water volume passed through macroporous α -Al₂O₃ ceramics (1), macroporous ceramics modified with AlOOH (2) and AlOOH/Ag (3).

The results obtained indicate a significant increase in the bacterial removal (inactivation) efficiency from water by macroporous α -Al₂O₃ ceramic samples after modification with AlOOH/Ag nanostructures. This increase in efficiency was caused by the presence of Ag in the composition of the modified ceramics. Ag is known to release Ag⁺ ions, which cause the inhibition of certain oxidative enzymes, protein denaturation, or interference with DNA replication [56].

As for efficiency compared to other materials, it should be noted that this will strongly depend on many factors, such as the initial bacterial load on the material, the flow rate, and the area and thickness of the filter. In our work, we adsorbed (inactivated) 5×10^6 bacterial cells per 1 cm² of material while ensuring 100% purification efficiency. For example, it was possible to retain about 10^5 bacterial cells per 1 cm² of material on Ti3C2/Al2O3/Ag/Cu-modified polypropylene fibers with a purification efficiency of 99.6% [57].

It should also be noted that, unlike previously obtained coatings on polymeric microfibers [42], ceramic composite filters can be regenerated by heat treatment and re-used.

4. Conclusions

Macroporous α -Al₂O₃ ceramics with a porosity of 75% and an average pore size of 187 microns were obtained. The impregnation of the ceramics with Al and Al/Ag nanoparticle suspensions, followed by the water oxidation of the nanoparticles fixed on the ceramic surface, resulted in the formation of nanostructured coatings which comprised boehmite nanosheets and boehmite nanosheets doped with silver nanoparticles, respectively. According to the hydrogen release kinetics in the process of nanoparticle oxidation, the amount of the boehmite nanosheets fixed in macroporous ceramics was determined as 1.1–1.5 wt.%. It was found that, for the filtration dynamic mode of water via macroporous ceramics modified with nanostructures, an increase in the efficiency of *S. aureus* removal from 76 to 98% was achieved.

Author Contributions: Conceptualization, A.S.L.; methodology, E.I.S., A.S.L. and O.V.B.; software, A.S.B.; validation, M.G.K.; formal analysis, E.I.S. and S.O.K.; investigation, S.O.K. and E.I.S.; resources, A.S.L. and A.S.B.; data curation, M.G.K. and A.S.B.; writing—original draft preparation, A.S.L. and O.V.B.; writing—review and editing, A.S.L. and O.V.B.; visualization, S.O.K. and A.S.B.; supervision, A.S.L.; project administration, A.S.L.; funding acquisition, A.S.L. All authors have read and agreed to the published version of the manuscript.

Funding: The work was performed according to the Government research assignment for ISPMS SB RAS, project FWRW-2022-0002 and of 2022's "Ecolan M-1.9" R&D Plan of the Russian–Vietnamese Tropical Research and Technological Center.

Institutional Review Board Statement: Not applicable.

Informed Consent Statement: Not applicable.

Data Availability Statement: Not applicable.

Acknowledgments: The XRD analyses were carried out with the equipment of Tomsk Regional Core Shared Research Facilities Center of National Research Tomsk State University. The center was supported by the Ministry of Science and Higher Education of the Russian Federation Grant no. 075-15-2021-693 (no. 13.RFC.21.0012).

Conflicts of Interest: The authors declare no conflict of interest.

References

1. Ohji, T.; Fukushima, M. Macro-porous ceramics: Processing and properties. *Int. Mater. Rev.* **2013**, *57*, 115–131. [\[CrossRef\]](#)
2. Zhu, J.B.; Yan, H. Microstructure and properties of mullite-based porous ceramics produced from coal fly ash with added Al₂O₃. *Int. J. Miner. Metall. Mater.* **2017**, *24*, 309–315. [\[CrossRef\]](#)
3. Samaei, S.M.; Gato Trinidad, S.; Altaee, A. The application of pressure-driven ceramic membrane technology for the treatment of industrial wastewaters—A review. *Sep. Purif. Technol.* **2018**, *200*, 198–220. [\[CrossRef\]](#)
4. Bodhak, S.; Nath, S.; Basu, B. Friction and wear properties of novel HDPE—HAp—Al₂O₃ biocomposites against alumina counterface. *J. Biomater. Appl.* **2009**, *23*, 407–433. [\[CrossRef\]](#) [\[PubMed\]](#)
5. Shumilov, V.; Kirilin, A.; Tokarev, A.; Boden, S.; Schubert, M.; Hampel, U.; Hupa, L.; Salmi, T.; Murzin, D.Y. Preparation of γ -Al₂O₃/ α -Al₂O₃ ceramic foams as catalyst carriers via the replica technique. *Catal. Today* **2022**, *383*, 64–73. [\[CrossRef\]](#)
6. Li, F.; Huang, X.; Liu, J.X.; Zhang, G.J. Sol-gel derived porous ultra-high temperature ceramics. *J. Adv. Ceram.* **2020**, *9*, 1–16. [\[CrossRef\]](#)
7. Zhang, M.; Li, X.; Zhang, M.; Xiu, Z.; Li, J.G.; Li, J.; Xie, M.; Chen, J.; Sun, X. High-strength macro-porous alumina ceramics with regularly arranged pores produced by gel-casting and sacrificial template methods. *J. Mater. Sci.* **2019**, *54*, 10119–10129. [\[CrossRef\]](#)
8. Lopez-Robledo, M.J.; Gómez-Martín, A.; Ramírez-Rico, J.; Martínez-Fernández, J. Sliding wear resistance of porous biomorphic ceramic. *Int. J. Refract. Hard. Met.* **2016**, *59*, 26–31. [\[CrossRef\]](#)
9. Zou, H.; Li, X.; Zhang, C.; Wen, Y.; Fan, Y.; Liu, Y.; Xiong, L.; Zheng, X.; Yang, J. Reactive synthesis for porous TiAlC ceramics by TiH₂, V, Al and graphite powders. *Ceram. Int.* **2021**, *47*, 28288–28295. [\[CrossRef\]](#)
10. Fadli, A.; Alfarisi, C.D. Recent Research and Development in Porous Alumina Ceramics for Biomedical Applications. In Proceedings of the Seminar Nasional Teknik Kimia Indonesia 2012, Jakarta, Indonesia, 20–21 September 2012; Department of Chemical Engineering, Riau University: Pekanbaru, Indonesia, 2012.
11. Piconi, C.; Maccauro, G.; Muratori, E.; Brach del Prever, E. Alumina и zirconia ceramics in joint substitutes: A review. *J. Appl. Biomater.* **2003**, *1*, 19–32.
12. Huang, S.-C.; Huang, C.-T.; Lu, S.Y.; Chou, K.S. Ceramic/polyaniline composite porous membranes. *J. Porous Mater.* **1999**, *6*, 153–159. [\[CrossRef\]](#)
13. Suzuki, T.A. Dense cell culture system for microorganisms using a stirred ceramic membrane reactor incorporating asymmetric porous ceramic filters. *J. Ferment. Bioeng.* **1996**, *82*, 264–271. [\[CrossRef\]](#)
14. Chou, K.-S.; Kao, K.B.; Huang, C.D.; Chen, C.Y. Coating and characterization of titania membrane on porous ceramic supports. *J. Porous Mater.* **1999**, *6*, 217–225. [\[CrossRef\]](#)
15. Colombo, P. Conventional and novel processing methods for cellular ceramics. *Philos. Trans. Royal Soc. A* **2006**, *364*, 109–124. [\[CrossRef\]](#)
16. Zender, H.; Leistner, H.; Searle, H.R. ZrO₂ materials for application in the ceramic industry. *Inter. Ceram. Rev.* **1990**, *39*, 33–36.
17. Gauckler, L.J.; Waeber, M.M.; Conti, C.; Jacobduliere, M. Ceramic foam for molten-metal filtration. *Met. J.* **1985**, *37*, 47–50. [\[CrossRef\]](#)
18. Terauchi, N.; Ohtani, T.; Yamanaka, K.; Tsuji, T.; Sudou, T.; Ito, K. Studies on a biological filter for musty odor removal in drinking water treatment processes. *Water Sci. Technol.* **1995**, *31*, 229–235. [\[CrossRef\]](#)

19. Jayasinghe, S.N.; Edirisinghe, M.J. A Novel method of forming open cell ceramic foam. *J. Porous Mater.* **2002**, *9*, 265–273. [[CrossRef](#)]
20. Wenzel, C.; Aneziris, G.C.; Tsetsekou, A.A. Study on application of silicon carbide filters for water purification. In Proceedings of the 10th ECerS Conference, Berlin, Germany, 17–21 June 2007; Göller Verlag: Baden-Baden, Germany, 2007; pp. 2073–2078, ISBN 3-87264-022-4.
21. Fuse, T.; Kobayashi, N.; Hasatani, M. Combustion characteristics of ethanol in a porous ceramic burner and ignition improved by enhancement of liquid fuel intrusion in the pore with ultrasonic irradiation. *Exp. Therm. Fluid Sci.* **2005**, *29*, 467–476. [[CrossRef](#)]
22. Garcia, E.; Osendi, M.I.; Miranzo, P. Thermal diffusivity of porous cordierite ceramic burners. *J. Appl. Phys.* **2002**, *92*, 2346–2349. [[CrossRef](#)]
23. Vakifahmetoglu, C.; Zeydanli, D.; Colombo, P. Porous polymer derived ceramics. *Mater. Sci. Eng. R Rep.* **2016**, *106*, 1–30. [[CrossRef](#)]
24. Yang, Y.; Kim, K.H.; Ong, J.L. A review on calcium phosphate coatings produced using a sputtering process—An alternative to plasma spraying. *Biomaterials* **2005**, *26*, 327–337. [[CrossRef](#)]
25. Sandhyarani, M.; Rameshbabu, N.; Venkateswarlu, K.; Rama Krishna, L. Fabrication, characterization and in-vitro evaluation of nanostructured zirconia/hydroxyapatite composite film on zirconium. *Surf. Coat. Technol.* **2014**, *238*, 58–67.
26. Bosetti, M.; Vernè, E.; Ferraris, M.; Ravaglioli, A.; Cannas, M. In vitro characterisation of zirconia coated by bioactive glass. *Biomaterials* **2001**, *22*, 987–994. [[CrossRef](#)]
27. Zhang, B.; Kwok, C.T.; Cheng, F.T.; Man, H.C. Fabrication of nano-structured HA/CNT coatings on Ti6Al4V by electrophoretic deposition for biomedical applications. *J. Nanosci. Nanotechnol.* **2011**, *11*, 10740–10745. [[CrossRef](#)] [[PubMed](#)]
28. Rauscher, M.D.; Boyne, A.; Dregia, S.A.; Akbar, S.A. Self-assembly of pseudoperiodic arrays of nanoislands on YSZ-(001). *Adv. Mater.* **2008**, *20*, 1699–1705. [[CrossRef](#)]
29. Ansari, H.M.; Dixit, V.; Zimmerman, L.B.; Rauscher, M.D.; Dregia, S.A.; Akbar, S.A. Self assembly of nanoislands on YSZ-(001) surface: A mechanistic approach toward a robust process. *Nano Lett.* **2013**, *29*, 2116–2121. [[CrossRef](#)]
30. Parikh, K.S.; Rao, S.S.; Ansari, H.M.; Zimmerman, L.B.; Lee, L.J.; Akbar, S.A.; Winter, J.O. Ceramic nanopatterned surfaces to explore the effects of nanotopography on cell attachment. *Mater. Sci. Eng. C Mater. Biol. Appl.* **2012**, *32*, 2469–2475. [[CrossRef](#)]
31. Ciobanu, C.S.; Iconaru, S.L.; Le Coustumer, P.; Constantin, L.V.; Predoi, D. Antibacterial activity of silver-doped hydroxyapatite nanoparticles against gram-positive and gram-negative bacteria. *Nanoscale Res. Lett.* **2012**, *7*, 324. [[CrossRef](#)]
32. Ciobanu, C.S.; Massuyeau, F.; Constantin, L.V.; Predoi, D. Structural and physical properties of antibacterial Ag-doped nano-hydroxyapatite synthesized at 100 °C. *Nanoscale Res. Lett.* **2011**, *6*, 613. [[CrossRef](#)]
33. Farooq, S.A.; Raina, A.; Mohan, S.; Arvind Singh, R.; Jayalakshmi, S.; Irfan Ul Haq, M. Nanostructured Coatings: Review on Processing Techniques, Corrosion Behaviour and Tribological Performance. *Nanomaterials* **2022**, *12*, 1323. [[CrossRef](#)]
34. Gu, Y.; Xia, K.; Wu, D.; Mou, J.; Zheng, S. Technical characteristics and wear-resistant mechanism of nano coatings: A review. *Coatings* **2020**, *10*, 233. [[CrossRef](#)]
35. Colombo, P.; Vakifahmetoglu, C.; Costacurta, S. Fabrication of ceramic components with hierarchical porosity. *J. Mater. Sci.* **2010**, *45*, 5425–5455. [[CrossRef](#)]
36. Lv, Y.; Liu, H.; Wang, Z.; Liu, S.; Hao, L.; Sang, Y.; Liu, D.; Wang, J.; Boughton, R.I. Silver nanoparticle-decorated porous ceramic composite for water treatment. *J. Membr. Sci.* **2009**, *331*, 50–56. [[CrossRef](#)]
37. Bhanushali, S.; Sastry, M. Strategies, challenges, and advancement in immobilizing silver nanomaterials. In *Immobilization Strategies: Biomedical, Bioengineering and Environmental Applications*; Tripathi, A., Savio Melo, J., Eds.; Springer: Singapore, 2021; pp. 597–643.
38. Hubadillah, S.K.; Tai, Z.S.; Othman, M.H.D.; Harun, Z.; Jamalludin, M.R.; Rahman, M.A.; Jaafar, J.; Ismail, A.F. Hydrophobic ceramic membrane for membrane distillation: A mini review on preparation, characterization, and applications. *Sep. Purif. Technol.* **2019**, *217*, 71–84. [[CrossRef](#)]
39. AbdulKadir, W.A.F.W.; Ahmad, A.L.; Seng, O.B.; Lah, N.F.C. Biomimetic hydrophobic membrane: A review of anti-wetting properties as a potential factor in membrane development for membrane distillation (MD). *J. Ind. Eng. Chem.* **2020**, *91*, 15–36. [[CrossRef](#)]
40. Dimitriadi, M.; Zafiropoulou, M.; Zinelis, S.; Silikas, N.; Eliades, G. Silane reactivity and resin bond strength to lithium disilicate ceramic surfaces. *Dent. Mater.* **2019**, *35*, 1082–1094. [[CrossRef](#)]
41. Aleksandr, L.; Alexander, P.; Olga, B.; Sergey, K.; Irena, G. Synthesis of antimicrobial AlOOH–Ag composite nanostructures by water oxidation of bimetallic Al–Ag nanoparticles. *RSC Adv.* **2018**, *8*, 36239–36244. [[CrossRef](#)]
42. Bakina, O.V.; Glazkova, E.A.; Lozhkomoiev, A.S.; Svarovskaya, N.V.; Rodkevich, N.G.; Lerner, M.I. Synthesis and antibacterial activity of cellulose acetate sheets modified with flower-shaped AlOOH/Ag. *Cellulose* **2020**, *27*, 6663–6676. [[CrossRef](#)]
43. Pervikov, A.V.; Suliz, K.V.; Lerner, M.I. Nanoalloying of clusters of immiscible metals and the formation of bimetallic nanoparticles in the conditions of non-synchronous explosion of two wires. *Powder Technol.* **2020**, *360*, 855–862. [[CrossRef](#)]
44. Lerner, M.I.; Glazkova, E.A.; Lozhkomoiev, A.S.; Svarovskaya, N.V.; Bakina, O.V.; Pervikov, A.V.; Psakhie, S.G. Synthesis of Al nanoparticles and Al/AlN composite nanoparticles by electrical explosion of aluminum wires in argon and nitrogen. *Powder Technol.* **2016**, *295*, 307–314. [[CrossRef](#)]
45. Lubarda, V.A. On the effective lattice parameter of binary alloys. *Mech. Mater.* **2003**, *35*, 53–68. [[CrossRef](#)]

46. Geisler, A.H.; Hill, J.K. Analyses and Interpretations of X-ray Diffraction Effects in Patterns of Aged Alloys. *Acta Cryst.* **1948**, *1*, 238–252. [[CrossRef](#)]
47. Emmanuelle, A.; Marquis, A. Reassessment of the Metastable Miscibility Gap in Al-Ag Alloys by Atom Probe Tomography. *Microsc. Microanal.* **2007**, *13*, 484–492.
48. Cheng, X.; Huang, X.; Wang, X.; Zhao, B.; Chen, A.; Sun, D. Phosphate adsorption from sewage sludge filtrate using zinc–aluminum layered double hydroxides. *J. Hazard. Mater.* **2009**, *169*, 958–964. [[CrossRef](#)] [[PubMed](#)]
49. Wang, D.Y.; Leuteritz, A.; Wang, Y.Z.; Wagenknecht, U.; Heinrich, G. Preparation and burning behaviors of flame retarding biodegradable poly (lactic acid) nanocomposite based on zinc aluminum layered double hydroxide. *Polym. Degrad. Stab.* **2010**, *95*, 2474–2480. [[CrossRef](#)]
50. Zhou, J.; Yang, S.; Yu, J.; Shu, Z. Novel hollow microspheres of hierarchical zinc–aluminum layered double hydroxides and their enhanced adsorption capacity for phosphate in water. *J. Hazard. Mater.* **2011**, *192*, 1114–1121. [[CrossRef](#)]
51. Bakina, O.V.; Kazantsev, S.O.; Pervikov, A.V.; Glazkova, E.A.; Svarovskaya, N.V.; Lozhkomoev, A.S.; Khorobraya, E.G. Structure, Morphology, and Antibacterial Properties of Mesoporous AlOOH–Metal Nanocomposites. *Inorg. Mater. Appl. Res.* **2021**, *12*, 767–775. [[CrossRef](#)]
52. Lozhkomoev, A.S.; Glazkova, E.A.; Bakina, O.V.; Lerner, M.I.; Gotman, I.; Gutmanas, E.Y.; Kazantsev, S.O.; Psakhie, S.G. Synthesis of core–shell AlOOH hollow nanospheres by reacting Al nanoparticles with water. *Nanotechnology* **2016**, *27*, 205603. [[CrossRef](#)]
53. Gai, W.Z.; Liu, W.H.; Deng, Z.Y.; Zhou, J.G. Reaction of Al powder with water for hydrogen generation under ambient condition. *Int. J. Hydrogen Energy* **2012**, *37*, 13132–13140. [[CrossRef](#)]
54. Kirfel, A.; Eichhorn, K. Accurate structure analysis with synchrotron radiation. The electron density in Al₂O₃ and Cu₂O. *Acta Crystallogr. Sect. A Found. Crystallogr.* **1990**, *4*, 271–284. [[CrossRef](#)]
55. Lozhkomoev, A.S.; Lerner, M.I.; Tsukanov, A.A.; Kazantsev, S.O.; Bakina, O.V.; Psakhie, S.G. On the possibility of soft matter nanostructure formation based on mesoporous aluminum hydroxide. Prospects for biomedical applications. *Phys. Mesomech.* **2017**, *20*, 134–141. [[CrossRef](#)]
56. Nakamura, S.; Sato, M.; Sato, Y.; Ando, N.; Takayama, T.; Fujita, M.; Ishihara, M. Synthesis and application of silver nanoparticles (Ag NPs) for the prevention of infection in healthcare workers. *Int. J. Mol. Sci.* **2019**, *20*, 3620. [[CrossRef](#)]
57. Jakubczak, M.; Karwowska, E.; Rozmysłowska-Wojciechowska, A.; Petrus, M.; Woźniak, J.; Mitrzak, J.; Jastrzębska, A.M. Filtration Materials Modified with 2D Nanocomposites—A New Perspective for Point-of-Use Water Treatment. *Materials* **2021**, *14*, 182. [[CrossRef](#)]